Soil cation storage as a key control on the timescales of carbon dioxide removal through enhanced weathering

Authors: Y. Kanzaki[1], N.J. Planavsky[2,3], S. Zhang[4], J. Jordan[5], C.T. Reinhard[1*]

Affiliations:

[1]School of Earth and Atmospheric Sciences, Georgia Institute of Technology, Atlanta, GA, USA.
[2]Department of Earth and Planetary Sciences, Yale University, New Haven, CT, USA.
[3]Yale Center for Natural Carbon Capture, New Haven, CT, USA.
[4]Department of Oceanography, Texas A&M, College Station, TX, USA.
[5]Porecast Research, LLC, Lawrence, KS, USA.

[*]corresponding author: chris.reinhard@eas.gatech.edu

Key Points:

- Cation storage in soils can temporarily undo the carbon dioxide removal that occurs during the enhanced weathering process.

- Lags in carbon removal after carbonate or silicate weathering can vary from years to many decades.

- Carbon removal lags should be quantified in enhanced weathering deployments through rigorous validation of models with real-world data.

Abstract: Significant interest and capital are currently being channeled into techniques for durable carbon dioxide removal (CDR) from Earth's atmosphere. A particular class of these approaches — referred to as enhanced weathering (EW) — seeks to modify the surface alkalinity budget to durably store CO_2 as dissolved inorganic carbon species. Here, we use SCEPTER — a reaction-transport code designed to simulate EW in managed lands — to evaluate the throughput and storage timescales of anthropogenic alkalinity in agricultural soils. Through a series of alkalinity flux simulations, we explore the main controls on cation storage and export from surface soils in key U.S. agricultural regions. We find that lag times between alkalinity modification and climate-relevant CDR can span anywhere from years to many decades, with background soil cation exchange capacity, agronomic target pH, and fluid infiltration all impacting the timescales of CDR relative to the timing of alkalinity input. There may be scope for optimization of weathering-driven alkalinity transport through variation in land management practice. However, there are tradeoffs with total CDR, optimal nutrient use efficiencies, and soil nitrous oxide (N_2O) fluxes that complicate attempts to perform robust time-resolved analysis of the net radiative impacts of CDR through EW in agricultural systems. Although CDR lag times will be more of an issue in some regions than others, these results have significant implications for the technoeconomics of EW and the integration of EW into voluntary carbon markets, as there may often be a large temporal disconnect between deployment of EW and climate-relevant CDR.

1. Introduction

Efforts to achieve key milestones aimed at limiting the extent of anthropogenic climate disruption in the coming century will very likely require significant amounts of net carbon dioxide removal (CDR) from Earth's atmosphere. Specifically, even optimistic scenarios for decarbonization of energy systems, transport, and industry in the coming decades still require roughly 1-10 gigatons of carbon dioxide (GtCO$_2$, 10^9 tons of CO$_2$) to be removed from the atmosphere each year by the end of the century to achieve net carbon neutrality [*IPCC*, 2018; *Rogelj et al.*, 2018]. The current supply of durable CDR — defined as carbon removal that is durable on timescale similar to or greater than the residence time of CO$_2$ in the atmosphere (~100 years) — is many orders of magnitude below this [*Smith et al.*, 2023]. There is thus strong impetus for rapid scaling of promising durable CDR approaches, and significant amounts of private and public funding flowing into efforts to develop the basic science underlying durable CDR pathways and bring them to scale.

Enhanced weathering (EW) is one particularly promising geochemical approach toward durable CDR. Enhanced weathering involves adding fine-grained cation-rich rock feedstocks (typically basalt, olivine, wollastonite, or steel slag) to soils, where they dissolve in the presence of elevated soil CO$_2$ to yield bicarbonate (HCO$_3^-$). This bicarbonate can in principle be transported by river/stream systems to the oceans, where much of it will remain stored on timescales on the order of 10^4 years [*Kanzaki et al.*, 2023b; *Lord et al.*, 2015; *Renforth and Henderson*, 2017]. Carbonate (limestone) weathering – currently in widespread use as an agricultural practice for soil pH management – can also lead to alkalinity export and CDR, although the efficiency and dynamics of this process are dependent in part on the pH at which weathering occurs [*Hamilton et al.*, 2007; *Oh and Raymond*, 2006]. Because it has the potential to leverage extensive existing agricultural infrastructure, requires relatively little energy beyond that required to transport feedstock, and may have a range of agronomic and socioeconomic co-benefits, EW has attracted considerable interest as a durable CDR pathway that has the potential to scale rapidly in a relatively cost-effective way [*Baek et al.*, 2023; *Beerling et al.*, 2020; *Beerling et al.*, 2018; *Calabrese et al.*, 2022].

However, there is a range of possible fates for cations released from EW feedstocks, including calcium carbonate or secondary clay mineral formation in terrestrial settings [*Bluth and Kump*, 1994; *Lal*, 2007], re-equilibration of the carbonic acid system in rivers and streams [*Harrington et al.*, 2023; *Knapp and Tipper*, 2022; *Zhang et al.*, 2022], and storage of cations on exchange sites within soils and in the lower critical zone [*Appelo*, 1994; *Bolt et al.*, 1976; *Spencer*, 1954]. In the case of (permanent) secondary mineral formation and carbonic acid system re-equilibration CO$_2$ is released back to the atmosphere, undoing the initial CDR. In the case of cation storage CDR is instead delayed for an exchange timescale, as cation storage in soils is ultimately reversible and released cations will be charge balanced by HCO$_3^-$ production upon release from the soil exchange complex (an exception to this may be EW using limestone as a feedstock, which could in some cases result in transient net CO$_2$ release rather than delayed CO$_2$ removal).

Methods are currently being developed for tracking the initial release of cations from EW feedstocks [e.g., *Reershemius et al.*, 2023]. These approaches can provide an estimate of the "CDR potential" that will eventually emerge assuming no downstream cation removal or CO$_2$ degassing. However, the timescales over which this CDR potential will be realized are poorly known. This is critical for the technoeconomics of EW, because a ton of carbon removed immediately has more value than a ton of carbon removed in the future [e.g., *Fearnside et al.*, 2000; *Groom and Venmas*,

87 2023; *Richards*, 1997; *van Kooten et al.*, 2021]. As a result, offset purchase contracts using EW as
88 a pathway must either accurately discount lagged carbon removal *ex-ante* or have *ex-post*
89 guardrails for empirically verifying cation fluxes through the system over time. In either case,
90 timescales of cation lag that are sufficiently long could potentially render EW projects unworkable
91 for some voluntary carbon markets as currently structured.
92
93 Here, we use a reaction-transport code [*Kanzaki et al.*, 2023a; *Kanzaki et al.*, 2022] designed to
94 simulate enhanced weathering (EW) in managed lands to evaluate the throughput and storage
95 timescales of anthropogenic alkalinity in agricultural soils. Through a series of idealized alkalinity
96 flux simulations, we explore the main controls on cation storage and export from surface soils in
97 key U.S. agricultural regions. We find that carbon removal lags induced by transient cation storage
98 in soils can range from years to many decades — varying significantly across key agricultural
99 regions of the U.S. – and suggest that carbon removal lags due to cation storage need to be
100 considered in future EW research and deployment efforts. Lastly, we discuss the implications of
101 these results for deployment of EW on carbon markets and suggest potential strategies through
102 which background soil characteristics and deployment practice can both be leveraged to shorten
103 carbon removal lags.
104

2. Materials and Methods

2.1 A gridded dataset for simulated alkalinity modification in U.S. agricultural regions

107 We focus here on key agricultural regions of the coterminous United States, basing our analysis
108 on areas with a cropland fraction greater than 10% and gridded at a resolution of 1ºx1º. As
109 boundary conditions for the initialization and spin-up of our reaction-transport code we use a series
110 of gridded data products for runoff, mean annual air temperature (MAT), soil moisture,
111 aboveground net primary productivity (NPP), soil organic matter (SOM), fertilization rate, topsoil
112 pH, soil cation exchange capacity (CEC), and soil base saturation (**Fig. 1**). Observational data are
113 derived from the sources shown in **Table 1**. Soil pCO_2 was calculated as a function of net primary
114 production (NPP) and temperature according to the method of [*Gwiazda and Broecker*, 1994]
115 adapted and modified by [*Goddéris et al.*, 2010], [*Gaillardet et al.*, 2019], and [*Zeng et al.*, 2022].
116
117 The reaction-transport model used here is designed to track feedstock-specific alkalinity release
118 and cation/carbon biogeochemistry in managed soils [*Kanzaki et al.*, 2023a; *Kanzaki et al.*, 2022].
119 We adopt a model configuration that is essentially the same as that described in [*Kanzaki et al.*,
120 2023a], which consists of two solid species (bulk soil phase plus soil organic matter), one gaseous
121 species (CO_2), and an inclusive range of aqueous species for evaluating charge balance and soil
122 acid-base balance [*Kanzaki et al.*, 2022]. We use four tuning parameters to initialize the soil
123 column in each grid cell: (1) an aggregate cation exchange parameter ($K_{H/Na}$); (2) a dissolved Ca^{2+}
124 concentration at the upper boundary of the soil column, which is a convenient way of representing
125 historical agricultural liming; (3) an input flux of organic carbon (OC) to the soil; and (4) a time
126 constant for organic carbon turnover (**Fig. 2**). These parameters are tuned to match the observed
127 values for soil pH, base saturation, soil organic matter content, and soil pCO_2 (**Fig. 1**), with the
128 soil column in each grid cell being spun up for 10^5 years to achieve steady state prior to alkalinity
129 modification.
130
131

132 Following spinup and initialization, we conduct alkalinity modification experiments in which CaO
133 is added as a source of alkalinity to the system. CaO is chosen as a feedstock because the
134 dissolution and alkalinity release are extremely rapid – the approach is designed to remove the
135 time-dependent uncertainty in dissolution rates associated with dissolution of less labile (but more
136 readily deployed) feedstocks such as basalt or olivine, and to isolate the effects of cation exchange
137 on the timescales of CDR. In the simulations shown here, feedstock is added continuously and
138 mixed homogeneously down to a depth of 25cm. Feedstock addition rate is iteratively tuned to
139 reach a specified agronomic target pH (pH$_t$ = 7.0) after one year of application. In-silico agronomic
140 soil pH is calculated by the method described in [*Kanzaki et al.*, 2023a] as the bulk phase pH value
141 of simulated soil in 1 mM CaCl$_2$ solution, equilibrated at a 1:2.5 (g/cm^3) soil/solution ratio. The
142 model domain for all simulations is 50 cm, which for our purposes is expected to yield a
143 conservative (i.e., lower-bound) estimate of cation travel times through the soil column.
144

145 **2.2 CDR calculation methods**

146 We evaluate CDR over time in the simulated soil column using three metrics, each of which is
147 designed to correspond to a distinct set of techniques for measurement, reporting, and verification
148 (MRV) of CDR in enhanced weathering deployments. The first is scaled to the fraction of
149 feedstock that dissolves in the soil (CDR$_{diss}$):
150

$$\mathrm{CDR_{diss}} = \frac{\sum\limits_{\theta} \gamma_\theta \Delta J_\theta^{diss}}{\sum\limits_{\theta} \gamma_\theta \Delta J_\theta^{feed}} \quad , \tag{1}$$

151

152 where γ_θ is the molar ratio of potential CO$_2$ capture per unit dissolution of feedstock θ (e.g., γ_{CaO} =
153 2), J_θ^{feed} and J_θ^{diss} are deployment (spreading) and dissolution fluxes of feedstock θ (mol m^{-2} y^{-1}),
154 respectively, and Δ denotes the flux difference between scenarios with and without feedstock
155 deployment. Mechanistically, this metric corresponds to time-integrated solid-phase approaches
156 for tracking on-field rates of CDR [*Beerling et al.*, 2024; *Kantola et al.*, 2023; *Reershemius et al.*,
157 2023; *Reershemius and Suhrhoff*, 2023]. In short, these techniques rely on measuring mobile
158 cations and immobile elements in soil before and after feedstock application and using these
159 measurements to estimate loss of base cations from applied feedstock. It is important to emphasize
160 that these techniques do not track CDR directly, and instead provide an estimate of "potential"
161 CDR that will emerge over time once the base cations have been charge balanced by alkalinity
162 production [*Reershemius et al.*, 2023].
163

164 The second CDR metric employed here is scaled to the reduction of gaseous CO$_2$ exchange
165 between the soil column and the atmosphere (CDR$_{diff}$):
166

$$\mathrm{CDR_{diff}} = \frac{\Delta J_{CO_2} - \Delta J_{SOC}}{\sum\limits_{\theta} \gamma_\theta \Delta J_\theta^{feed}} \quad , \tag{2}$$

167

168 where γ_θ, J_θ^{feed}, and Δ are defined as above and J_{CO2} and J_{SOC} are the soil-atmosphere flux of CO$_2$
169 (mol m^{-2} y^{-1}) and the decomposition flux (mol m^{-2} y^{-1}) of soil organic carbon (SOC), respectively.
170 Mechanistically, this metric reflects a decrease in the flux of CO$_2$ from the soil column to the

171 atmosphere due to HCO_3^- production in the soil, and could in principle be measured through CO_2
172 gas fluxes from treated and control soils via eddy flux towers [*Baldocchi*, 2003], flux
173 chambers[*Pumpanen et al.*, 2004], or gas-phase CO_2 sensors[*Yasuda et al.*, 2007]. In contrast to
174 the solid-phase metric shown by Eq. (1), this metric tracks CDR directly and reflects additional
175 HCO_3^- production (and a corresponding reduction of the soil-atmosphere CO_2 flux) due to soil
176 management.

177

178 Lastly, we can scale CDR efficiency to the increase in advective fluxes of aqueous dissolved
179 inorganic carbon species through the soil column (CDR_{adv}):

180

$$\mathrm{CDR}_{\mathrm{adv}} = \frac{\Delta J_{DIC} - \Delta J_{SIC}}{\displaystyle\sum_{\theta} \gamma_\theta \Delta J_\theta^{feed}} \qquad , \tag{3}$$

181

182 Where γ_θ, J_θ^{feed}, J_{SIC}, and Δ are defined as above and J_{DIC} represents the flux (mol m^{-2} y^{-1}) of total
183 dissolved inorganic carbon (i.e., aqueous CO_2, HCO_3^-, and CO_3^{2-}) advected out of soil column.
184 Mechanistically, this metric reflects additional HCO_3^- production and advection out of the system
185 due to feedstock application and could in principle be measured by lysimeter techniques at the
186 field scale [*Weihermüller et al.*, 2007], point-collected dissolved solute measurements at the
187 catchment scale [*Larkin et al.*, 2022] , or possibly at larger scales through measurements of solute
188 composition in stream/river systems. Similar to Eq. (2), this metric directly tracks net CDR in the
189 soil column rather than gross alkalinity release.

190

191 Note that all of these metrics for CDR efficiency are referenced to the maximum potential CDR,
192 which assumes that all base cations released from feedstock θ are instantly and completed leached
193 upon deployment and charge-balanced only by production of bicarbonate ions. At steady state, the
194 reduction in soil-atmosphere CO_2 flux should be equivalent to the increase in bicarbonate
195 advection ($CDR_{diff} \sim CDR_{adv}$). In the case of negligible cation sinks (e.g., secondary carbonate or
196 silicate mineral phases) and on arbitrarily long timescales, $CDR_{diss} \sim CDR_{diff} \sim CDR_{adv}$. However,
197 transient cation storage could result in lag periods for which CDR_{diff} (or CDR_{adv}) < CDR_{diss}. This
198 allows us to isolate and quantify cation storage lags through time-dependent offsets between
199 CDR_{diss} and CDR_{diff}/CDR_{adv}.

200

201 **3. Results**

202 We first examine timescales of alkalinity release, cation exchange, and carbon removal in four
203 representative sites across major agricultural regions in the U.S.: (1) Site 128, located in the
204 Northern Plains region; (2) Site 311, located in the Corn Belt; (3) Site 161, located in the Southern
205 Plains region; and (4) Site 411, located in the Southeast (**Fig. 1, 2**). As expected, alkalinity release
206 into the system is effectively instantaneous across all sites (**Fig. 3**), with dissolution-based CDR
207 (CDR_{diss}) matching effective CDR potential (CDR_{eff}) on a timescale of days to weeks. Again, this
208 is by design, as our intent is to isolate exchange and transport lags from feedstock dissolution lags.
209 However, most of the alkalinity released from feedstock is initially stored as exchangeable calcium
210 (Ca_{exch}) and is only gradually released back into the system as an advective cation flux (Ca_{adv}) over
211 timescales ranging from years to decades (**Fig. 3**). This causes a significant lag in carbon removal
212 relative to alkalinity input because it is only when the exchangeable calcium is released into the
213 advective flux and charge balanced by HCO_3^- production that CDR can occur.

214
215   Although there is often a slight offset between carbon removal based on soil-atmosphere CO_2
216   exchange (CDR_{diff}) and advection of new DIC (CDR_{adv}) in the first decade, they, as expected, track
217   each other closely. These two metrics for carbon removal should be equivalent at steady state. The
218   timescales of actual carbon removal (tracked by both CDR_{diff} and CDR_{adv}) are significantly longer
219   than those of alkalinity release (tracked by CDR_{diss}) across all sites (**Fig. 3**). For example, for our
220   deployment in the Corn Belt CDR_{diff} and CDR_{adv} reach only ~40% of the effective CDR potential
221   after 10 years, with a timescale of ~50 years required to reach 80% of effective carbon removal
222   (**Fig. 3b**). In contrast, realized CDR reaches ~80% of its potential within the first decade after
223   deployment in the Southeast regional site (**Fig. 3d**).
224
225   Because the timescale required to achieve a particular threshold of CDR potential varies by region,
226   we geospatially analyze carbon removal lags across key agricultural regions in the U.S. (**Fig. 4**).
227   There are relatively few sites that show any tangible carbon removal in the first year despite
228   instantaneous cation and alkalinity input (**Fig. 4a**), and these are generally restricted to scattered
229   locations in the southeastern U.S. (Alabama, Georgia, and Florida; **Fig. 4e,i**). Most of the regions
230   examined here are below 50% of effective CDR potential after 5 years, and in some regions (the
231   Corn Belt and Great Plains) it takes well over 10 years after instantaneous cation and alkalinity
232   input for carbon removal to occur (**Fig. 4h,l**). Considering all regions together, it takes roughly 10
233   years to surpass a median carbon removal efficiency of 50%, with a median CDR efficiency of
234   75% surpassed in ~20 years (**Fig. 5d,g**). However, median lag times vary significantly by region
235   — for instance, in the Corn Belt median CDR lag is ~50 years to achieve 75% of CDR potential,
236   while the same carbon removal potential is achieved in the Southeast nearly an order of magnitude
237   more rapidly (**Fig. 5h,i**).
238
239   The magnitude of cation lag at any site clearly varies as a function of background soil
240   characteristics. This is evident, for example, in the Southeast sites which generally show
241   significantly shorter lag times overall as a result of very low cation exchange capacities with high
242   water fluxes (**Fig. 1h, 4f,j, 5f,i**). At the same time, soil management strategy can also significantly
243   impact cation lag times. For example, increasing agronomic target pH (pH_t) can result in
244   significantly higher CDR efficiency for a given time horizon (**Fig. 6**) because of gradual cation
245   loading on the soil exchange complex, which is more rapid at the higher alkalinity fluxes associated
246   with higher pH_t. The impact of this can be significant – in the case of Site 411, a value of $pH_t =$
247   5.5 results in an advective CDR efficiency of ~30% after ten years, while the same CDR efficiency
248   can be achieved in only ~2 years at $pH_t = 7.0$.
249
250   **4. Discussion**
251   Our results suggest that carbon dioxide removal lags induced by cation exchange in agricultural
252   soils can be significant, and in some cases can last multiple decades, adding to a robust evidence
253   base for the following key conclusions: (1) cation sorption in soils with low base saturation (the
254   ratio of cations to protons in soil sorption sites) will delay climate-relevant CO_2 removal in EW
255   deployments; (2) this lag time can be multiple years or even several decades; and (3) these lag
256   times will vary geographically and with management practice. However, it is important to stress
257   that although these basic conclusions are very likely robust, we do not currently have firm
258   constraints on the uncertainty in lag times for any individual region or deployment strategy, and
259   there is a pressing need to validate model estimates of carbon removal lag against real-world

260   observations. As a result, we would strongly argue that given the current state of knowledge
261   reaction-transport models are not equipped to provide robust estimates of CDR lag for ready
262   inclusion in carbon accounting schemes [e.g., *Balmford et al.*, 2023].

263

264   Our time lag estimates may be conservative, given that our lag estimates are based on simulations
265   with a 50 cm vertical domain and soil thickness throughout agricultural regions of the U.S. is
266   significantly greater than this [e.g., *Pelletier et al.*, 2016], such that the overall alkalinity input
267   required to saturate the soil exchange complex would be larger. On the other hand, it is expected
268   that there will be a certain length scale at which soils will become diffusionally isolated from the
269   atmosphere. This isolation length scale will very likely vary with soil type and seasonally, which
270   combine to drive time-dependent changes to soil moisture and fluid saturation. In addition, the
271   apparent role of target pH in enhancing or inhibiting cation and alkalinity throughput (**Fig. 6**) could
272   be complicated by implementation of more realistic feedstock dissolution kinetics. There is a well-
273   known scaling between ambient soil pH and rates of feedstock dissolution [e.g., *Kump et al.*, 2000;
274   *Snaebjörnsdóttir et al.*, 2020], such that there should be a tradeoff between more effective cation
275   throughput when target pH is continuously maintained at a high value and less effective feedstock
276   dissolution. This dynamic represents an important topic for future research.

277

278   An extended carbon removal lag after weathering induced by soil cation exchange has several
279   significant implications for deployment of EW in a market framework. Most importantly, the
280   economic value of carbon removal is time-varying, which means that EW deployments that aim
281   to sell carbon offsets on a voluntary market should be able to accurately quantify the timing of
282   climate-relevant CDR across timescales. One reasonable conclusion would be that suppliers of
283   EW-based offsets on a voluntary market should be expected to either confront the technical
284   challenge of quantifying carbon removal lags prior to deployment or the challenges to project
285   finance associated with empirically verifying carbon removal over extended timescales prior to
286   receiving revenue for offset production. The structure of carbon marketplaces could also be
287   modified to account for this feature of the EW pathway. In any case, our results suggest that cation
288   storage is ubiquitous and needs to be considered in any EW deployment.

289

290   There is significant potential scope for optimizing the efficiency of alkalinity transport through
291   soils via both deployment siting and land management practice. For instance, our idealized
292   deployment scheme – in particular, continuously managing soil pH at a uniform optimal
293   agronomic value – is not optimized for cation transit through the soil column and from a land
294   management perspective is also unlikely to be pursued in practice. Pulsed alkalinity addition
295   followed by cation flushing with strong acid from fertilizer application may increase the efficiency
296   of alkalinity transport in managed soils. However, one would expect lower time-integrated CDR
297   overall, along with higher time-integrated soil N_2O fluxes [*Blanc-Betes et al.*, 2020; *Chiaravalloti*
298   *et al.*, 2023; *Kantola et al.*, 2023; *Val Martin et al.*, 2023; *Wang et al.*, 2021b], in scenarios in
299   which pH is intentionally and repeatedly lowered to enhance cation flushing. Additionally, in
300   large-scale interpolated soil databases there are some regions that show increased pH and base
301   cation abundance in the exchange complex at depth [e.g., *Poggio et al.*, 2021]. In some cases, these
302   gradients may enhance local alkalinity export. In any case, there are currently large uncertainties
303   in quantifying the tradeoffs and overall impacts of optimized alkalinity throughput on agricultural
304   greenhouse gas budgets, and this represents a critical topic for future research.

305

306 Perhaps most importantly, our results highlight the need for more empirical constraints on cation
307 and alkalinity throughput in managed lands. Accurate representation of the soil exchange complex
308 in process-based models such as that explored here is challenging, and there is currently significant
309 uncertainty in the dynamics of cation breakthrough in managed soils that are well out of steady
310 state. Moving forward, the production of large datasets that can constrain cation fluxes and carbon
311 removal lag times, some of which could be produced by private-sector suppliers of carbon removal
312 through EW, would represent a major step forward in our ability to accurately quantify cation
313 storage across a range of scenarios and deployment strategies. There is a pressing need for these
314 data to be rigorously and transparently evaluated, and for the results to be leveraged in the
315 development of process-based models of soil cation exchange and time-dependent charge balance
316 dynamics.
317

318 **5. Conclusions**

319 Soil biogeochemical modeling suggests that cation exchange dynamics in agricultural soils can
320 lead to significant lags between alkalinity input from EW feedstocks (weathering) and climate-
321 relevant carbon dioxide removal. Lag times can vary from less than a year to many decades and
322 will be controlled by background soil characteristics and land management practice. In some cases,
323 carbon removal lags can be reduced through thoughtful site selection and/or optimized soil pH
324 management. However, carbon removal lags induced by soil cation storage should be ubiquitous
325 in the field, and EW deployments that commodify carbon removal through charge balance must
326 take storage-induced removal lags into account. In the near-term, this will require rigorous and
327 transparent validation of reaction-transport models against real-world observations of alkalinity
328 throughput in managed lands.
329

337 **Author contributions:**
338   Conceptualization: YK, CTR, NJP
339   Methodology: YK, SZ, CTR, NJP
340   Investigation: YK, SZ, CTR, NJP
341   Visualization: YK, CTR, NJP
342   Funding acquisition: CTR, NJP
343   Project administration: CTR, NJP
344   Supervision: CTR, NJP
345   Writing – original draft: CTR, YK
346   Writing – review & editing: YK, CTR, NJP, SZ, JJ

347 **Competing interests:** JJ is employed by Mati Carbon, A B-Corp owned by the not-for-profit organization
348   Swaniti Initiative.
349

350

351

352

References:

Appelo, C. A. J. (1994), Cation and proton exchange, pH variations, and carbonate reactions in a freshening aquifer, *Water Resources Research*, *30*, 2793-2805.

Baek, S. H., Y. Kanzaki, J. M. Lora, N. J. Planavsky, C. T. Reinhard, and S. Zhang (2023), Impact of climate on the global capacity for enhanced rock weathering on croplands, *Earth's Future*, *11*.

Baldocchi, D. D. (2003), Assessing the eddy covariance technique for evaluating carbon dioxide exchange rates of ecosystems: past, present and future, *Global Change Biology*, *9*, 479-492.

Balmford, A., S. Keshav, F. Venmans, D. A. Coomes, B. Groom, A. Madhavapeddy, and T. Swinfield (2023), Realizing the social value of impermanent carbon credits, *Nature Climate Change*, *13*, 1172-1178.

Beerling, D. J., et al. (2024), Enhanced weathering in the US Corn Belt delivers carbon removal with agronomic benefits, *Proceedings of the National Academy of Sciences, USA*, *121*, doi:10.1073/pnas.2319436121.

Beerling, D. J., et al. (2020), Potential for large-scale CO2 removal via enhanced rock weathering with croplands, *Nature*, *583*, 242-248.

Beerling, D. J., et al. (2018), Farming with crops and rocks to address global climate, food and soil security, *Nature Plants*, *4*, 138-147.

Blanc-Betes, E., I. B. Kantola, N. Gomez-Casanovas, M. D. Hartman, W. J. Parton, A. L. Lewis, D. J. Beerling, and E. H. DeLucia (2020), In silico assessment of the potential of basalt amendments to reduce N2O emissions from bioenergy crops, *GCB Bioenergy*, *13*, 224-241.

Bluth, G. J. S., and L. R. Kump (1994), Lithologic and climatologic controls of river chemistry, *Geochimica et Cosmochimica Acta*, *58*, 2341-2359.

Bolt, G. H., M. G. M. Bruggenwert, and A. Kamphorst (1976), Adsorption of cations by soil, in *Developments in Soil Science*, edited by G. H. Bolt and M. G. M. Bruggenwert, pp. 54-90.

Calabrese, S., B. Wild, M. B. Bertagni, I. C. Bourg, C. White, F. Aburto, G. Cipolla, L. V. Noto, and A. Porporato (2022), Nano- to global-scale uncertainties in terrestrial enhanced weathering, *Environmental Science & Technology*, doi:10.1021/acs.est.2c03163.

Chiaravalloti, I., N. Theunissen, S. Zhang, J. Wang, F. Sun, A. A. Ahmed, E. Pihlap, C. T. Reinhard, and N. J. Planavsky (2023), Mitigation of soil nitrous oxide emissions during maize production with basalt amendments, *Frontiers in Climate*, *5*.

Fearnside, P. M., D. A. Lashof, and P. Moura-Costa (2000), Accounting for time in mitigating global warming through land-use change and forestry, *Mitigation and Adaptation Strategies for Global Change*, *5*, 239-270.

Fick, S. E., and R. J. Hijmans (2017), WorldClim 2: new 1km spatial resolution climate surfaces for global land areas *International Journal of Climatology*, *37*, 4302-4315.

Gaillardet, J., D. Calmels, G. Romero-Mujalli, E. Zakharova, and J. Hartmann (2019), Global climate control on carbonate weathering intensity, *Chemical Geology*, *527*.

Goddéris, Y., J. Z. Williams, J. Schott, D. Pollard, and S. L. Brantley (2010), Time evolution of the mineralogical composition of Mississippi Valley loess over the last 10 kyr: Climate and geochemical modeling, *Geochimica et Cosmochimica Acta*, *74*, 6357-6374.

Groom, B., and F. Venmas (2023), The social value of offsets, *Nature*, *619*, 768-773.

392 Gwiazda, R. H., and W. S. Broecker (1994), The separate and combined effects of temperature, soil pCO2, and organic
393 acidity on silicate weathering in the soil environment: Formulation of a model and results, *Global Biogeochemical*
394 *Cycles*, *8*, 141-155.

395 Hamilton, S. K., A. L. Kurzman, C. Arango, L. Jin, and G. P. Rovertson (2007), Evidence for carbon sequestration by
396 agricultural liming, *Global Biogeochemical Cycles*, *21*.

397 Harrington, K. J., R. G. Hilton, and G. Henderson (2023), Implications of the riverine response to enhanced weathering
398 for CO2 removal in the UK, *Applied Geochemistry*, *152*.

399 IPCC (2018), Global Warming of 1.5ºC. An IPCC Special Report on the impacts of global warming of 1.5ºC above
400 pre-industrial levels and related global greenhouse gas emission pathways, in the context of strengthening the global
401 response to the threat of climate change, sustainable development, and efforts to eradicate poverty*Rep.*, In press.

402 Kantola, I. B., et al. (2023), Improved net carbon budgets in the US Midwest through direct measured impacts of
403 enhanced weathering, *Global Change Biology*, *29*, 7012-7028.

404 Kanzaki, Y., I. Chairavalloti, S. Zhang, N. J. Planavsky, and C. T. Reinhard (2023a), In-silico calculation of soil pH
405 by SCEPTER v1.0, *Geoscientific Model Development*, *In review*, doi:10.5194/gmd-2023-137.

406 Kanzaki, Y., N. J. Planavsky, and C. T. Reinhard (2023b), New estimates of the storage permanence and ocean co-
407 benefits of enhanced rock weathering, *PNAS Nexus*, *2*.

408 Kanzaki, Y., S. Zhang, N. J. Planavsky, and C. T. Reinhard (2022), Soil Cycles of Elements simulator for Predicting
409 TERrestrial regulation of greenhouse gases: SCEPTER v0.9, *Geoscientific Model Development*, *15*, 4959-4990.

410 Knapp, W. J., and E. T. Tipper (2022), The efficacy of enhanced carbonate weathering for carbon dioxide
411 sequestration, *Frontiers in Climate*, *4*.

412 Kump, L. R., S. L. Brantley, and M. A. Arthur (2000), Chemical weathering, atmospheric CO2, and climate, *Annual*
413 *Review of Earth and Planetary Sciences*, *28*, 611-667.

414 Lal, R. (2007), Carbon management in agricultural soils, *Mitigation and Adaptation Strategies for Global Change*,
415 *12*, 303-322.

416 Larkin, C. S., et al. (2022), Quantification of CO2 removal in a large-scale enhanced weathering field trial on an oil
417 palm plantation in Sabah, Malaysia, *Frontiers in Climate*, *4*.

418 Lord, N. S., A. Ridgwell, M. C. Thorne, and D. J. Lunt (2015), An impulse response function for the "long tail" of
419 excess atmospheric CO2 in an Earth system model, *Global Biogeochemical Cycles*, *30*, 2-17.

420 Oh, N.-H., and P. A. Raymond (2006), Contribution of agricultural liming to riverine bicarbonate export and CO2
421 sequestration in the Ohio River basin, *Global Biogeochemical Cycles*, *20*.

422 Pan, B., S. K. Lam, E. S. Wang, A. Mosier, and D. Chen (2021), New approach for predicting nitrification and its
423 fraction of N2O emissions in global terrestrial ecosystems, *Environmental Research Letters*, *16*.

424 Pelletier, J. D., P. D. Broxton, P. Hazenberg, X. Zeng, P. A. Troch, G. Niu, Z. C. Williams, M. A. Brunke, and D.
425 Gochis (2016), Global 1-km gridded thickness of soil, regolith, and sedimentary deposit layers, edited by O. DAAC,
426 Oak Ridge, Tennessee, USA.

427 Poggio, L., L. M. DeSousa, N. H. Batjes, G. Heuvelink, B. Kempen, E. Ribiero, and D. Rossiter (2021), SoilGrids
428 2.0: Producing soil information for the globe with quantified spatial uncertainty, *Soil*, *7*, 217-240.

429   Pumpanen, J., et al. (2004), Comparison of different chamber techniques for measuring soil CO2 flux, *Agricultural*
430   *and Forest Meteorology*, *123*, 159-176.

431   Reershemius, T., et al. (2023), Initial validation of a soil-based mass-balance approach for empirical monitoring of
432   enhanced rock weathering rates, *Environmental Science & Technology*, *57*, 19497-19507.

433   Reershemius, T., and T. J. Suhrhoff (2023), On error, uncertainty, and assumptions in calculating carbon dioxide
434   removal rates by enhanced rock weathering in Kantola et al., 2023, *Global Change Biology*, *30*.

435   Reitz, M., W. E. Sanford, G. B. Senay, and J. Cazenas (2017), Annual estimates of recharge, quick-flow runoff, and
436   evapotranspiration for the contiguous US using empirical regression equations, *J Am Water Resour As*, *53*, 961-983.

437   Renforth, P., and G. Henderson (2017), Assessing ocean alkalinity for carbon sequestration, *Reviews of Geophysics*,
438   *55*, 636-674.

439   Richards, K. R. (1997), The time value of carbon in bottom-up studies, *Critical Reviews in Environmental Science*
440   *and Technology*, *27*, S279-S292.

441   Rodell, M., et al. (2004), The Global Land Data Assimilation System, *Bulletin of the American Meteorological Society*,
442   *85*, 381-394.

443   Rogelj, J., et al. (2018), Scenarios toward limiting global mean temperature increase below 1.5ºC, *Nature Climate*
444   *Change*, *8*, 325-332.

445   Smith, S. M., et al. (2023), The State of Carbon Dioxide Removal - 1st Edition*Rep.*

446   Snaebjörnsdóttir, S. O., B. Sigfússon, C. Marieni, D. Goldberg, S. R. GIslason, and E. H. Oelkers (2020), Carbon
447   dioxide storage through mineral carbonation, *Nature Reviews Earth & Environment*, *1*, 90-102.

448   Spencer, W. F. (1954), Influence of cation-exchange reactions on retention and availability of cations in sandy soils,
449   *Soil Science*, *77*, 129-136.

450   Tuanmu, M. N., and W. Jetz (2014), A global 1-km consensus land-cover product for biodiversity and ecosystem
451   modeling, *Global Ecology and Biogeography*, *23*, 1031-1045.

452   USDA (2011), RCA Appraisal 2011*Rep.*, Washington, DC.

453   Val Martin, M., et al. (2023), Improving nitrogen cycling in a land surface model (CLM5) to quantify soil N2O, NO,
454   and NH3 emissions from enhanced rock weathering with croplands, *Geoscientific Model Development*, *16*, 5783-
455   5801.

456   van Kooten, G. C., P. Withey, and C. M. T. Johnston (2021), Climate urgency and the timing of carbon fluxes, *Biomass*
457   *and Bioenergy*, *151*.

458   Walkinshaw, M., A. T. O'Geen, and D. E. Beaudette (2022), Soil Properties, California Soil Resource Lab, edited.

459   Wang, Y., J. Mao, M. Jin, F. M. Hoffman, X. Shi, S. D. Wullschleger, and Y. Dai (2021a), Development of
460   observation-based global multilayer soil moisture products for 1970 to 2016, *Earth System Science Data*, *13*, 4385-
461   4405.

462   Wang, Y., Z. Yao, Y. Zhan, X. Zheng, M. Zhou, G. Yan, L. Wang, C. Werner, and K. Butterbach-Bahl (2021b),
463   Potential benefits of liming to acid soils on climate change mitigation and food security, *Global Change Biology*, *27*,
464   2807-2821.

465   Weihermüller, L., J. Simens, M. Deurer, S. Knoblauch, H. Rupp, A. Göttlein, and T. Pütz (2007), In situ soil water
466   extraction: A review, *Journal of Environmental Quality*, *36*, 1735-1748.

467   Yasuda, Y., Y. Ohtani, Y. Mizoguchi, T. Nakamura, and H. Miyahara (2007), Development of a CO2 gas analyzer
468   for monitoring soil CO2 concentrations, *Journal of Forest Research*, *13*, 320-325.

469   Zeng, S., G. Kaufmann, and Z. Liu (2022), Natural and anthropogenic driving forces of carbonate weathering and the
470   related carbon sink flux: a model comparison study at global scale, *Global Biogeochemical Cycles*, *36*.

471   Zhang, S., N. J. Planavsky, J. A. R. Katchinoff, P. A. Raymond, Y. Kanzaki, T. Reershemius, and C. T. Reinhard
472   (2022), River chemistry constraints on the carbon capture potential of surficial enhanced rock weathering, *Limnology
473   and Oceanography*, doi:10.1001/lno.12244.

474   Zhao, M., F. A. Heinsch, R. R. Nemani, and S. W. Running (2005), Improvements of the MODIS terrestrial gross and
475   net primary production global data set, *Remote Sensing of Environment*, *95*, 164-176.
476
477
478
479
480
481
482
483
484
485
486
487
488
489
490
491
492
493
494
495
496
497
498
499
500
501
502
503
504
505
506
507
508
509
510
511
512

513 **TABLES**

514

515 **Table 1.** Sources of observational data for model spin-up and tuning.

Parameter	Observational Dataset
Temperature	[*Fick and Hijmans*, 2017]
Soil moisture	[*Wang et al.*, 2021a]
Runoff/infiltration	[*Reitz et al.*, 2017]
Soil pH	[*Poggio et al.*, 2021]
Soil organic matter	[*Poggio et al.*, 2021]
Cation exchange capacity	[*Walkinshaw et al.*, 2022]
Nitrification rate	[*Pan et al.*, 2021]
Base saturation	[*Poggio et al.*, 2021]
Soil erosion	[*USDA*, 2011]
Soil porosity	[*Rodell et al.*, 2004]
Cropland fraction	[*Tuanmu and Jetz*, 2014]
Net primary production (NPP)	[*Zhao et al.*, 2005]

516
517
518
519
520
521
522
523
524
525
526
527
528
529
530
531
532
533
534
535
536
537
538
539
540
541
542
543
544
545
546
547
548
549
550
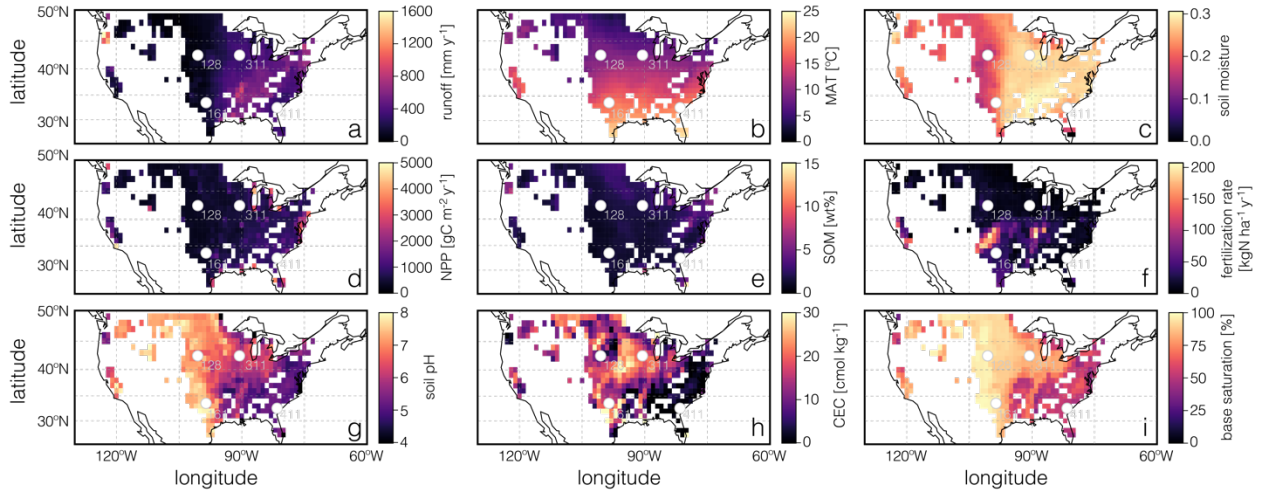
FIGURES:

Figure 1. Gridded input data and boundary conditions from the coterminous U.S. used in our reaction-transport model. Key input parameters include runoff (a), mean annual air temperature (MAT; b), soil moisture (c), above ground net primary production (NPP; d), soil organic matter (SOM; e), fertilization rate (f), initial soil pH (g), soil cation exchange capacity (CEC; h), and soil base saturation (i). Also shown are the four site locations discussed in the text (open circles), labelled by site number.
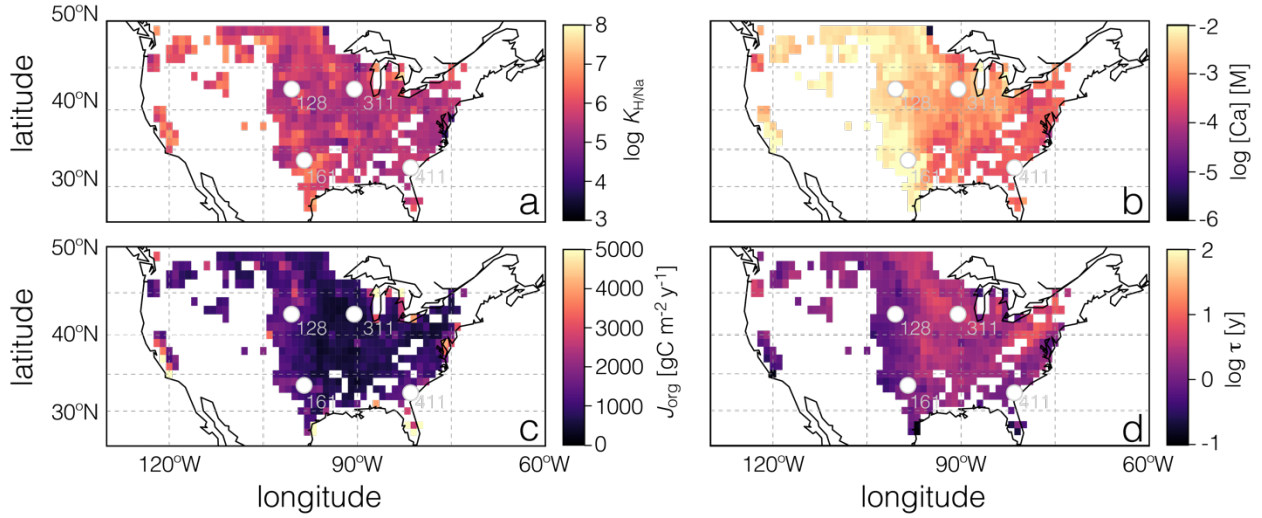
Figure 2. Results for gridded tuned parameters obtained during model spinup. Shown are soil cation exchange cofficients ($K_{H/Na}$; a), soil surface dissolved calcium concentrations ([Ca]; b), organic carbon fluxes to the soil surface (J_{org}; c), and turnover times for soil organic carbon (t; d). Also shown are the four site locations discussed in the text (open circles), labelled by site number.
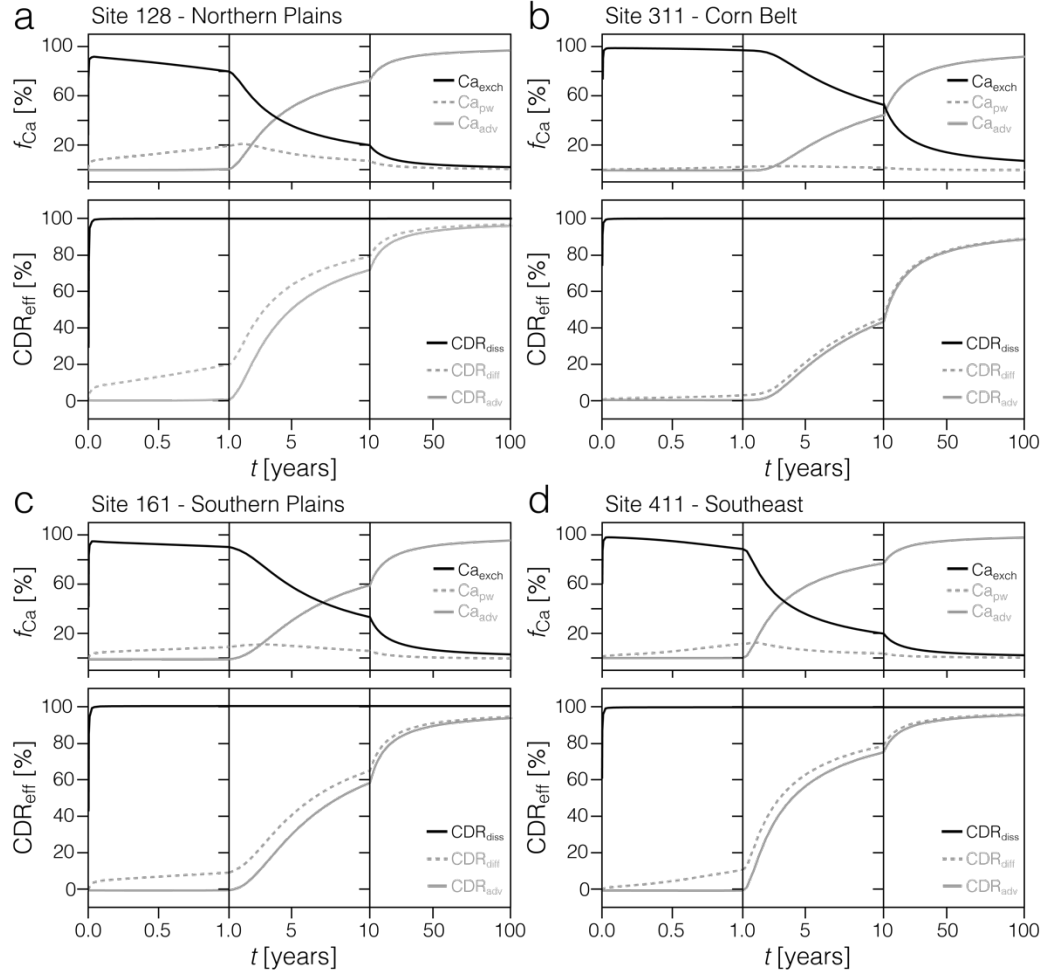
Figure 3. Time-dependent cation and CO_2 removal dynamics for the four sites discussed in the text. The upper panel for each site shows the relative distribution of calcium (Ca), the primary cation tracer in our simulations, between dissolved porewater Ca (Ca_{pw}), exchangeable Ca (Ca_{exch}), and Ca advecting through the soil column (Ca_{adv}). The lower panel for each site shows the carbon dioxide removal efficiency relative to perfect (stoichiometric) removal (CDR_{eff}) according to three CDR metrics — tracking dissolution of the solid phase (CDR_{diss}), tracking changes in soil CO_2 diffusion (CDR_{diff}), and tracking advection of dissolved inorganic carbon (DIC) out of the model domain (CDR_{adv}).
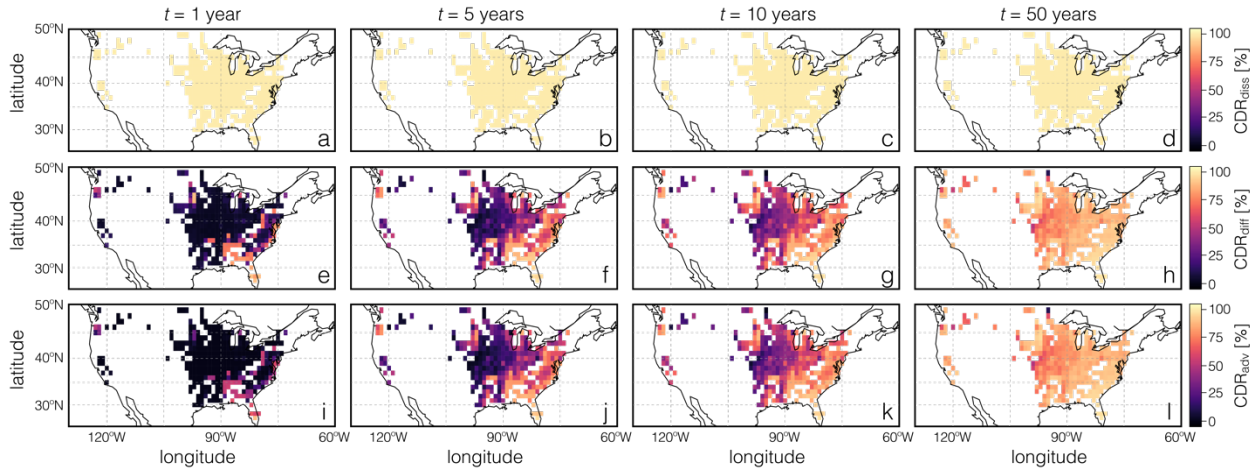
Figure 4. Regional variability in carbon dioxide removal efficiency relative to stoichiometric removal (CDR_{eff}) over time. Shown from left to right are cumulative CDR_{eff} values for time horizons of 1, 5, 10, and 50 years from the start of feedstock application. (a-d) CDR_{eff} values relative to fractional feedstock dissolution (CDR_{diss}); (e-h) CDR_{eff} values relative to changes in soil CO_2 diffusion (CDR_{diff}). (i-l) CDR_{eff} values relative to changes in the advection of dissolved inorganic carbon (DIC) out of the model domain (CDR_{adv}).
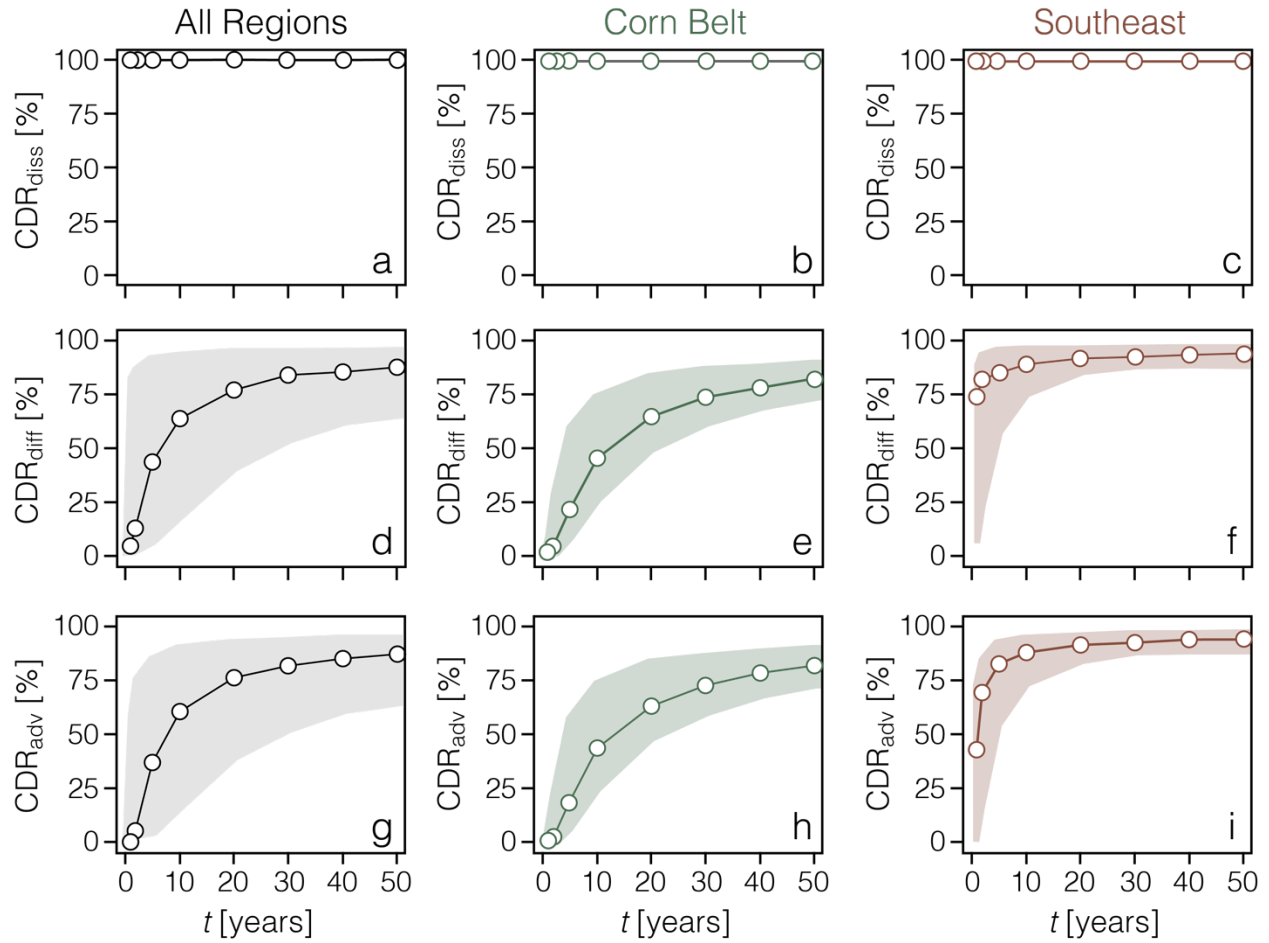
Figure 5. Aggregated regional CDR efficiency (CDR$_{eff}$) over time. Median values (open circles) and 95% confidence intervals (shaded envelopes) are shown for all U.S. grid cells examined here (left), aggregated Corn Belt grid cells (middle), and aggregated grid cells from the Southeastern U.S. (right). Values are shown relative to solid feedstock dissolution (CDR$_{diss}$; a-c), changes in soil CO_2 diffusion (CDR$_{diff}$; d-f), and changes in advection of dissolved inorganic carbon (DIC) out of the model domain (CDR$_{adv}$; g-i).
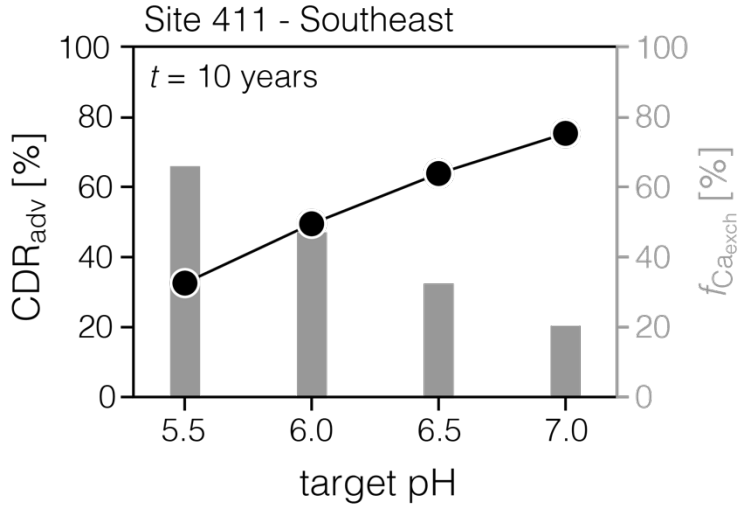
Figure 6. Example simulations from Site 411 (Southeast region) showing the impact of agronomic target pH on the fraction of calcium in the exchangeable pool ($f_{Ca,exch}$) and advective CDR efficiency (CDR_{adv}) over time. All results are shown for a time horizon of 10 years after initial alkalinity modification. Increasing agronomic target pH results in more rapid shift in base saturation of the soil exchange complex, reducing the timescale required to achieve a given CDR efficiency.